CHAPTER 4

Stator Flux Vector Control of Doubly-Fed Induction Generator using Back-to-Back Two-Level Voltage Source Converter

4.1 Introduction

This chapter presents a DFIG using back-to-back two-level voltage source converter, which based on the vector control technique. The rotor-side converter is controlled using stator flux vector control technique and the grid-side converter is controlled using grid voltage vector control technique.

This chapter is organized as follows. Section 4.2 presents the DFIG system and dynamic mathematical model of DFIG. Section 4.3 proposes the stator flux vector controller for rotor-side converter in DFIG system. Simulation results are shown in Section 4.4, Finally, conclusion is drawn in Section 4.5.

4.2 Doubly-fed induction generator system and mathematical model

A typical configuration of a DFIG system is illustrated in Figure 4.1. It uses a wound rotor induction machine with slip rings. The DFIG is an excellent choice as a small hydro turbine because its stator of the generator can be connected directly to the utility grid even though the mechanical angular speed can be changed with the prevailing velocity while the rotor-side connected to the grid is though the back-to-back converter, grid filter, and transformer, respectively, on its dc side to a grid-side converter which transmits the rotor slip frequency power to frequency of utility grid. A transformer is usually needed to step up the low voltage of the voltage source converter to utility grid voltage.

A control scheme of the DFIG using back-to-back converter is proposed. The objective of the control scheme for the rotor-side converter ensures decoupling control of the stator active and reactive powers drawn from the utility grid. The control scheme for the grid-side converter is to keep the dc-link voltage constant and make available reactive power to the grid when required. This control strategy generally leads to good transient behavior and acceptable steady-state operation. It operates at a constant switching frequency, which makes the use of advanced modulation techniques possible. Therefore, it becomes easier to optimize conversion power losses or to simplify the grid filter design.

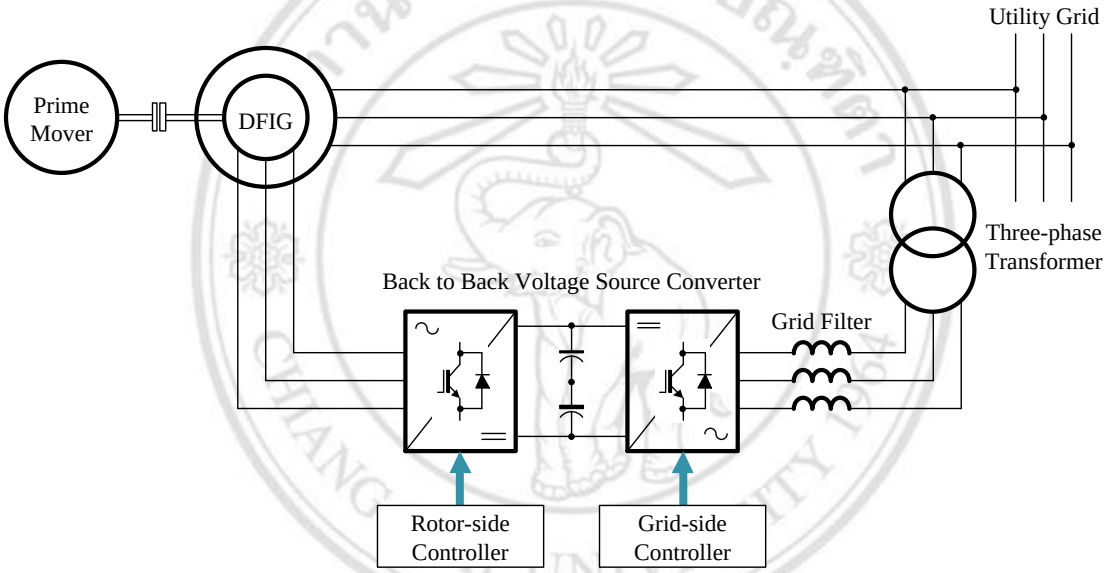

Figure 4.1 Configuration for the DFIG system using back-to-back converter.

4.2.1 Dynamic modeling of the doubly-fed induction generator

The dynamic models of the DFIG are presented considering the state of the art related to this field. The equivalent circuit of a DFIG can be expressed in different reference frames such as the stationary reference frame, the rotor reference frame, or the synchronous reference frame fixed to either the stator voltage [10], [47] or the stator flux [11], [48]. A general expression of the direct and quadrant axes equivalent circuits of the DFIG in rotating reference frame are shown in Figure 4.2.

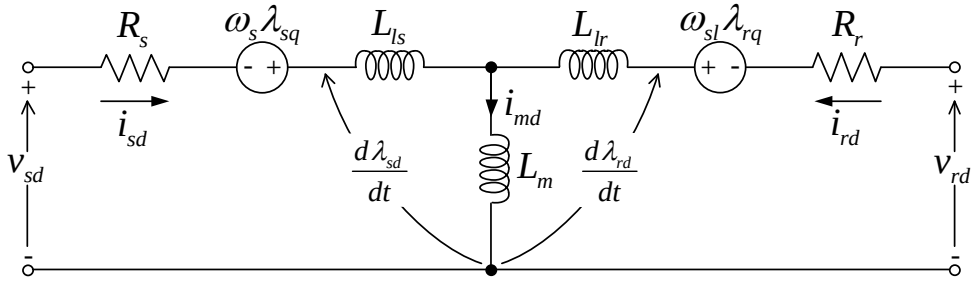

(a) Direct axis (*d*-axis)

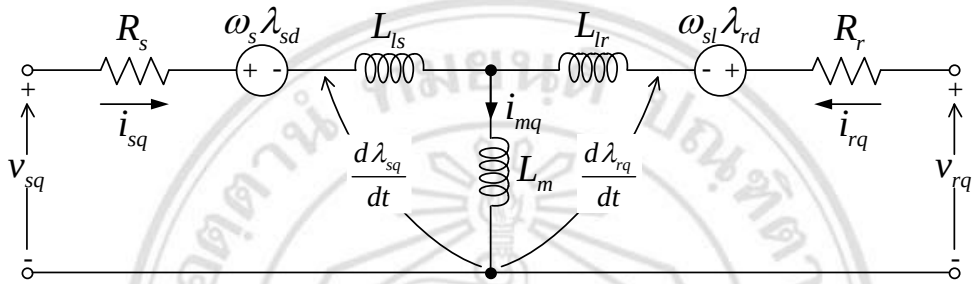

(b) Quadrate axis (*q*-axis)

Figure 4.2 Equivalent circuit of the DFIG in rotating reference frame.

The complete mathematical model voltage equations of the DFIG in the rotating reference frame, where the iron losses and end-effects cannot be normally neglected, are represented as follows

$$\begin{cases} v_{sd} = R_s i_{sd} + \dfrac{d\lambda_{sd}}{dt} - \omega_s \lambda_{sq}, \\ v_{sq} = R_s i_{sq} + \dfrac{d\lambda_{sq}}{dt} + \omega_s \lambda_{sd}, \\ v_{rd} = R_r i_{rd} + \dfrac{d\lambda_{rd}}{dt} - (\omega_s - \omega_r)\lambda_{sq}, \\ v_{rq} = R_r i_{rq} + \dfrac{d\lambda_{rq}}{dt} - (\omega_s - \omega_r)\lambda_{sd}, \end{cases} \tag{4.1}$$

where s, r are stator and rotor indices, d, q are direct and quadrate indices for orthogonal components, $v_{sd}, v_{sq}, v_{rd}, v_{rq}$ are the direct and quadrate stator and rotor voltages, $i_{sd}, i_{sq}, i_{rd}, i_{rq}$ are the direct and quadrate stator and rotor currents, $\lambda_{sd}, \lambda_{sq}, \lambda_{rd}, \lambda_{rq}$ are the direct and quadrate stator and rotor flux

linkages, R_s, R_r are the stator and rotor phase resistances, and $\omega_s, \omega_r, \omega_{sl}$ are the synchronous angular speed, the rotor angular speed, and the slip angular speed $(\omega_{sl} = \omega_s - \omega_r)$.

The stator and rotor flux linkage components can be expressed as

$$\begin{cases} \lambda_{sd} = (L_{ls} + L_m) i_{sd} + L_m i_{rd} = L_s i_{sd} + L_m i_{rd}, \\ \lambda_{sq} = (L_{ls} + L_m) i_{sq} + L_m i_{rq} = L_s i_{sq} + L_m i_{rq}, \\ \lambda_{rd} = (L_{lr} + L_m) i_{rd} + L_m i_{sd} = L_r i_{rd} + L_m i_{sd}, \\ \lambda_{rq} = (L_{lr} + L_m) i_{rq} + L_m i_{sq} = L_r i_{rq} + L_m i_{sq}, \end{cases} \tag{4.2}$$

where L_s is the stator phase inductance $(L_{ls} + L_m)$, L_r is the rotor phase inductance $(L_{lr} + L_m)$, and L_m is the magnetizing phase inductance.

The electromagnetic torque T_e produced by the DFIG can be written in terms of the rotating reference frame as

$$\begin{cases} \\ T_e = \dfrac{3}{2} p_p \left(i_{sq} \lambda_{sd} - i_{sd} \lambda_{sq} \right), \\ = \dfrac{3}{2} p_p L_m \left(i_{sq} i_{rd} - i_{sd} i_{rq} \right), \\ = \dfrac{3}{2} p_p \dfrac{L_m}{L_r} \left(i_{sq} \lambda_{rd} - i_{sd} \lambda_{rq} \right), \end{cases} \tag{4.3}$$

where T_e is the electromagnetic torque and p_p is number of pole pairs.

Neglecting the power losses associated with the stator resistances, the active and reactive stator powers are given by

$$\begin{cases} P_s = \dfrac{3}{2} \left(v_{sd} i_{sd} + v_{sq} i_{sq} \right), \\ Q_s = \dfrac{3}{2} \left(v_{sq} i_{sd} - v_{sd} i_{sq} \right). \end{cases} \tag{4.4}$$

Similarly, the rotor powers (also called slip power) can be calculated as

$$\begin{cases} P_r = \frac{3}{2}\left(v_{rd}i_{rd} + v_{rq}i_{rq}\right), \\ Q_r = \frac{3}{2}\left(v_{rq}i_{rd} - v_{rd}i_{rq}\right). \end{cases} \tag{4.5}$$

where P_s, Q_s are the stator active and reactive powers and P_r, Q_r are the rotor active and reactive powers.

4.2.2 Power flow and operation modes of DFIG

A DFIG can transmit power to the utility grid through both the generator stator and the converters. Considering that power flowing out of the DFIG is negative, works as generator mode, the power distribution for the DFIG able to work as a generator in both sub-synchronous and super-synchronous operation. It is indicated by the operating rotor speed at below and above synchronous speed as shown in Figure 4.3. For the generator operates in the sub-synchronous speed, the slip is positive, which the rotor-side of the DFIG will absorb power from the utility grid through the converters, whereas the generator operates in the super-synchronous speed, the slip is negative, the rotor power will be delivered from the rotor-side through the converters to the utility grid [49].

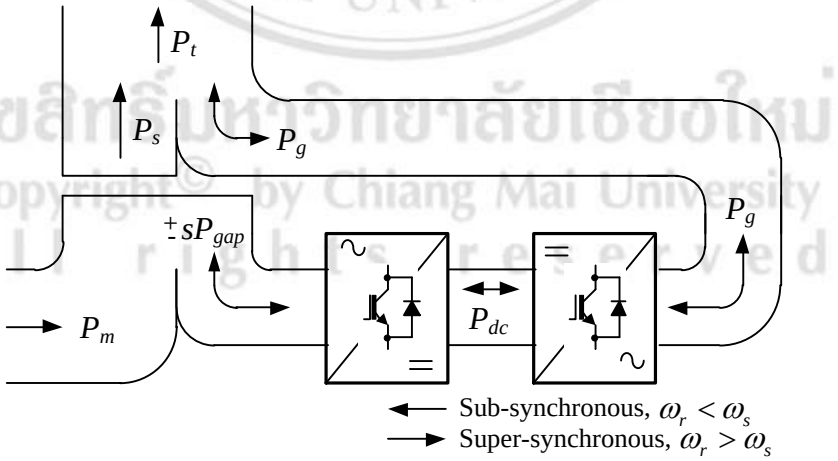

Figure 4.3 Power flow diagram of a DFIG.

Assume the converter is able to control the power flow at the grid-side converter at any time so its reactive power is zero. This assumption is

reasonable because the converter rating is at almost maximum 30% of the generator rating and it is used primarily for supplying the active power of the rotor to the utility grid. Therefore, the reactive power exchanged between the DFIG and the utility grid is equal to the reactive power in the stator $Q_t = Q_s$. The reactive power from the stator will be zero in case of a strong power system or when there is no requirement for the DFIG control ability of the voltage. In this case, the DFIG supplies only active power and is magnetized through the rotor, with the power factor of the DFIG close to unity. Otherwise, the reactive power set-point of the DFIG will be defined for the voltage control purpose [50].

The active power from the rotor is proportional to the slip s of the DFIG multiply by the air-gap power P_{gap} , $P_r = -sP_{gap}$. However, for high power machines the stator resistance is neglected, also the air-gap power is the stator power. By definition, the rotor active power P_r is given by

$$P_r = -sP_s, \tag{4.6}$$

the slip s is defined as

$$s = \frac{\omega_s - \omega_r}{\omega_s}. \tag{4.7}$$

When the power losses in the converters are neglected, the active power transmitted to the utility grid is the sum of stator active power P_s and rotor active power P_r then the rotor power add up to the grid-side power converter P_g . The total active power P_t of system can be derived as.

$$P_t = P_s + P_g, \tag{4.8}$$

where P_t is the total active power and P_g is the grid-side active power.

4.3 Rotor-side converter controlled using stator flux vector control

4.3.1 Stator flux vector control principle

The vector control technique developed for induction machines [51] can be applied to doubly-fed induction machines [11]. Traditionally, the techniques to control the rotor-side converter of DFIG system are the stator flux vector control, which reference frame has to be aligned with the stator flux linkage, which decouples the rotor currents into stator active and reactive power components and adjusts them separately in stator fluxed reference frame [11], [52].

The stator flux vector control is achieved by aligning the *d*-axis of the rotating reference frame. Therefore, the stator voltage equations in *d-q* rotating reference frame can be expressed as

$$v_{sd} = 0,\ v_{sq} = |v_s|, \tag{4.9}$$

where v_{sd} and v_{sq} are the stator voltage components in rotating reference frame.

Indicating the orientation of *d*-axis reference frame aligned in the stator flux vector, the following relationships are obtained [11],

$$\begin{cases} |\lambda_s| = \lambda_{sd} = L_m i_{md},\ \ \lambda_{sq} = 0, \\ \lambda_{rd} = \sigma L_r i_{rd},\ \ \lambda_{rq} = \sigma L_r i_{rq} + \dfrac{L_m^2}{L_s} i_m. \end{cases} \tag{4.10}$$

where $\sigma = 1 - \dfrac{L_m^2}{L_s L_r}$.

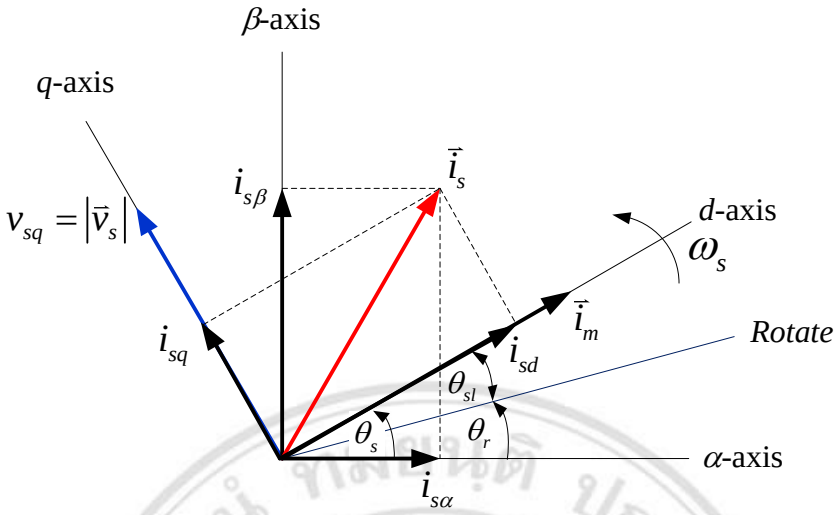

Figure 4.4 Vector diagram between the stationary reference frame and stator flux vector reference frame.

Figure 4.4 shows a relationship between the stationary reference frame and stator flux vector reference frame for the DFIG. The voltage equations of the DFIG in (4.1) is applied to stator flux orientation the relationship between the torque and the voltages and currents in *d*-*q* rotating reference frame can be written as

$$\begin{cases} v_{sd} = R_s i_{sd}, \\ v_{sq} = R_s i_{sq} + \omega_s L_m i_{md}, \\ v_{rd} = R_r i_{rd} + \sigma L_r \dfrac{d}{dt} i_{rd} - \omega_{sl} \sigma L_r i_{rq}, \\ v_{rq} = R_r i_{rq} + \sigma L_r \dfrac{d}{dt} i_{rq} + \omega_{sl} \left(\sigma L_r i_{rq} - \dfrac{v_{sq} L_m}{\omega_s L_s} \right). \end{cases} \tag{4.11}$$

The electromagnetic torque T_e equation in terms of the rotor current is given by

$$T_e = -\frac{3}{2} p_p \frac{L_m}{\omega_s L_s} v_{sq} i_{rq}. \tag{4.12}$$

From (4.12), the electromagnetic torque of DFIG can be controlled by the *q*-axis rotor current component. Considering (4.4), neglecting the power losses

associated with the stator resistance and under stator flux orientation, the stator active and reactive power are given by

$$\begin{cases} P_s = \dfrac{3}{2} v_{sq} i_{sq} = -\dfrac{3}{2} \dfrac{L_m}{L_s} v_{sq} i_{rq}, \\ Q_s = \dfrac{3}{2} v_{sq} i_{sd} = \dfrac{3}{2} \dfrac{L_m}{L_s} v_{sd} \left(i_{md} - i_{rd} \right). \end{cases} \tag{4.13}$$

4.3.2 Stator flux vector position

The stator flux vector control technique of DFIG required determining the stator flux vector position θ_s, which can be obtained from the stator flux linkage in $\alpha\beta$ stationary reference frame as

$$\theta_s = \tan^{-1}\left(\frac{\lambda_{s\beta}}{\lambda_{s\alpha}} \right). \tag{4.14}$$

The stator flux linkage in stationary reference frame $\lambda_{s\alpha}, \lambda_{s\beta}$ can be calculated from the stator voltage equations as

$$\begin{cases} \lambda_{s\alpha} = \int \left(v_{s\alpha} - R_s i_{s\alpha} \right) dt, \\ \lambda_{s\beta} = \int \left(v_{s\beta} - R_s i_{s\beta} \right) dt. \end{cases} \tag{4.15}$$

This method requires an integrator, which is replaced by a band-pass filter or low-pass filter. The drawbacks of the determination of the stator flux based on stator voltage equation are small offsets/dc drift and saturation problems.

In this thesis, an improved stator flux angle calculation with grid-flux orientation technique is employed [53]. A simple method using the measured stator/grid voltage and a phase-locked loop (PLL) to derive the stator flux position,

$$\theta_s = \theta_g - \frac{\pi}{2}. \tag{4.16}$$

From the above equation, the stator flux vector position angle can be calculated by subtracting 90° phase shift from the grid voltage angle. This technique is a simple but it is necessary to measure the grid voltage and is not essential to know machine parameters.

4.3.3 Stator flux vector control scheme

The structure of rotor-side converter control in stator flux vector control is shown in Figure 4.5. The current control loops implement the effective control of the stator active and reactive powers of the DFIG. The stator active and reactive powers are independently regulated by the decoupled rotor current controllers in *d*-*q* rotating reference frame. The *d*-*q* axis rotor current references i_{rd}^*, i_{rq}^* are calculated by

$$\begin{cases} i_{rd}^* = -\dfrac{2}{3}\dfrac{L_s}{v_{sq}L_m}Q_s^* + \dfrac{v_{sq}}{\omega_s L_m}, \\ i_{rq}^* = -\dfrac{2}{3}\dfrac{\omega_s L_s}{v_{sq}L_m p_p}T_e^*. \end{cases} \tag{4.17}$$

The measured generator speed ω_r is used to compute the desired electromagnetic torque reference T_e^*, which is controlled by the power converters. The electromagnetic torque reference T_e^* is produced by the *q*-axis rotor current component reference i_{rq}^*. The stator reactive power can be controlled by the stator reactive power reference Q_s^*, which is calculated according to (4.14). It is generated by the *d*-axis rotor current component reference i_{rd}^*. The rotor current references i_{rd}^*, i_{rq}^* are compared to the measured rotor current i_{rd}, i_{rq}, giving is the error rotor currents which are the inputs of PI rotor current controllers. Next, the outputs of the rotor current controllers are the voltage references in the rotating reference frame

v^*_{Lrd}, v^*_{Lrq}. The compensations correspond to the rotor voltage signals and the decoupling terms of the *d-q* axis rotor current components. Therefore, the reference rotor voltages v^*_{rd}, v^*_{rq} are expressed as

$$\begin{cases} v^*_{rd} = v^*_{Lrd} - \omega_{sl}\sigma L_r i_{rq}, \\ v^*_{rq} = v^*_{Lrq} + \omega_{sl}\left(\sigma L_r i_{rd} - \dfrac{v_{sq}L_m}{\omega_s L_s}\right). \end{cases} \tag{4.18}$$

The reference rotor voltages v^*_{rd}, v^*_{rq} are transformed to the *abc* reference frame. Finally, the PWM signals is generated by the SVPWM technique, which generated switching signals for rotor-side two-level VSC.

The grid-side converter is controlled to maintain the constant dc-link voltage and to provides the reactive power to the utility grid. The control scheme and PI controller design of the grid-side converter will be discussed in Chapter 5.

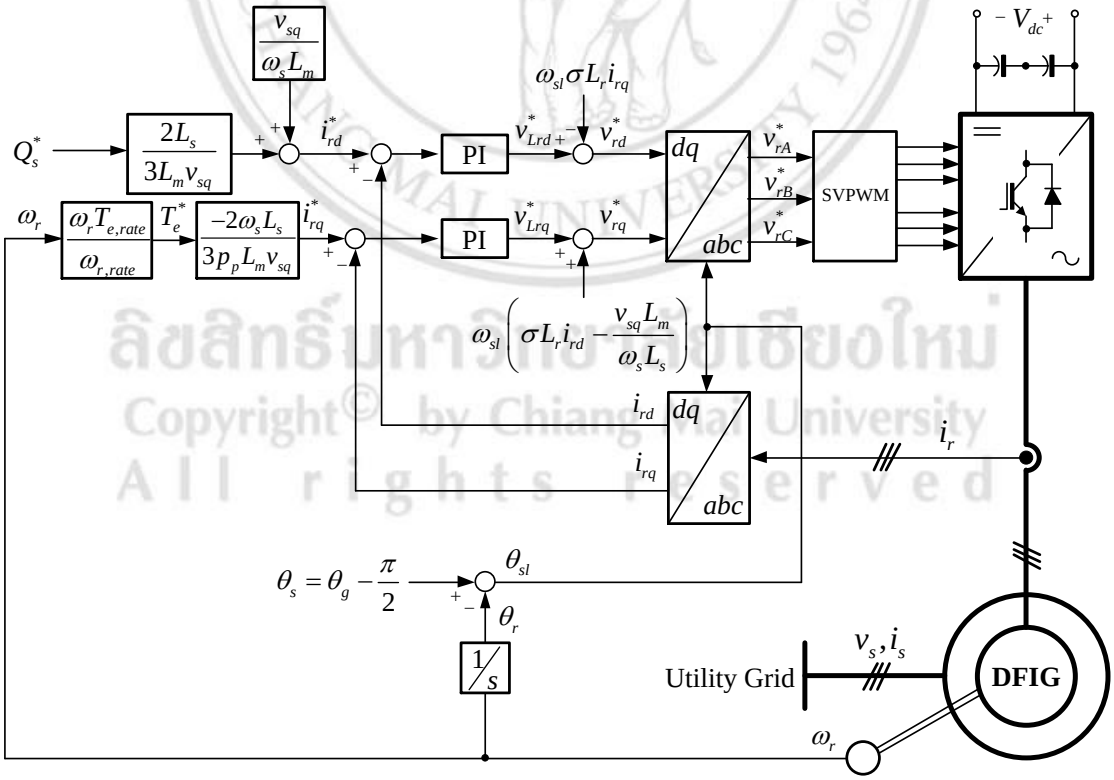

Figure 4.5 Block diagram of rotor-side two-level VSC of DFIG system with the stator flux vector control.

4.4 Simulation results

Simulations of the stator flux vector control scheme for a 1kW DFIG system have been developed using Matlab/Simulink in order to evaluate the performance. The parameters of the generator are shown in Table 2.1. The nominal dc-link voltage is 180 V, which is controlled by the dc-link voltage controller in the grid-side converter and SVPWM with a switching frequency of 4 kHz is used for the back-to-back two-level VSC. In order to evaluate the stator flux vector control scheme for DFIG system, the simulation has been carried out under the following conditions.

4.4.1 Dynamic response in sub-synchronous speed

Initial studies with sub-synchronous constant speed at 1200 rpm and reactive power steps is carried out to simulate the dynamic response of the stator flux vector control scheme. The stating speed is set to 1200 rpm, which is generated by the constant torque command T_e^* for constant stator active power P_s, and the stator reactive power reference Q_s^* is set to 0 VAR for unity power factor. The reactive power reference is changed from 0 VAR to +300 VAR at 1.0 s and from +300 to -300 VAR at 1.1 s, respectively. Simulation results are shown in Figure 4.6.

Figure 4.6 (a) shows the electromagnetic torque reference T_e^* and the electromagnetic torque of the generator T_e. It can be seen that the electromagnetic torque of generator is equal to the reference torque, around -3.5 Nm, which is operated at constant speed at 1200 rpm. Figure 4.7 (b) shows the rotor current reference components i_{rd}^*, i_{rq}^* and the measured rotor current components i_{rd}, i_{rq} in *d*-*q* rotating reference frame. As can be seen from Figure 4.6 (b), the *d*-axis rotor current i_{rd} follows the rotor current reference i_{rd}^*, while the *q*-axis rotor current i_{rq} is maintained at its constant reference value i_{rq}^*. The three-phase rotor currents in sub-synchronous speed are also shown in Figure 4.6 (c).

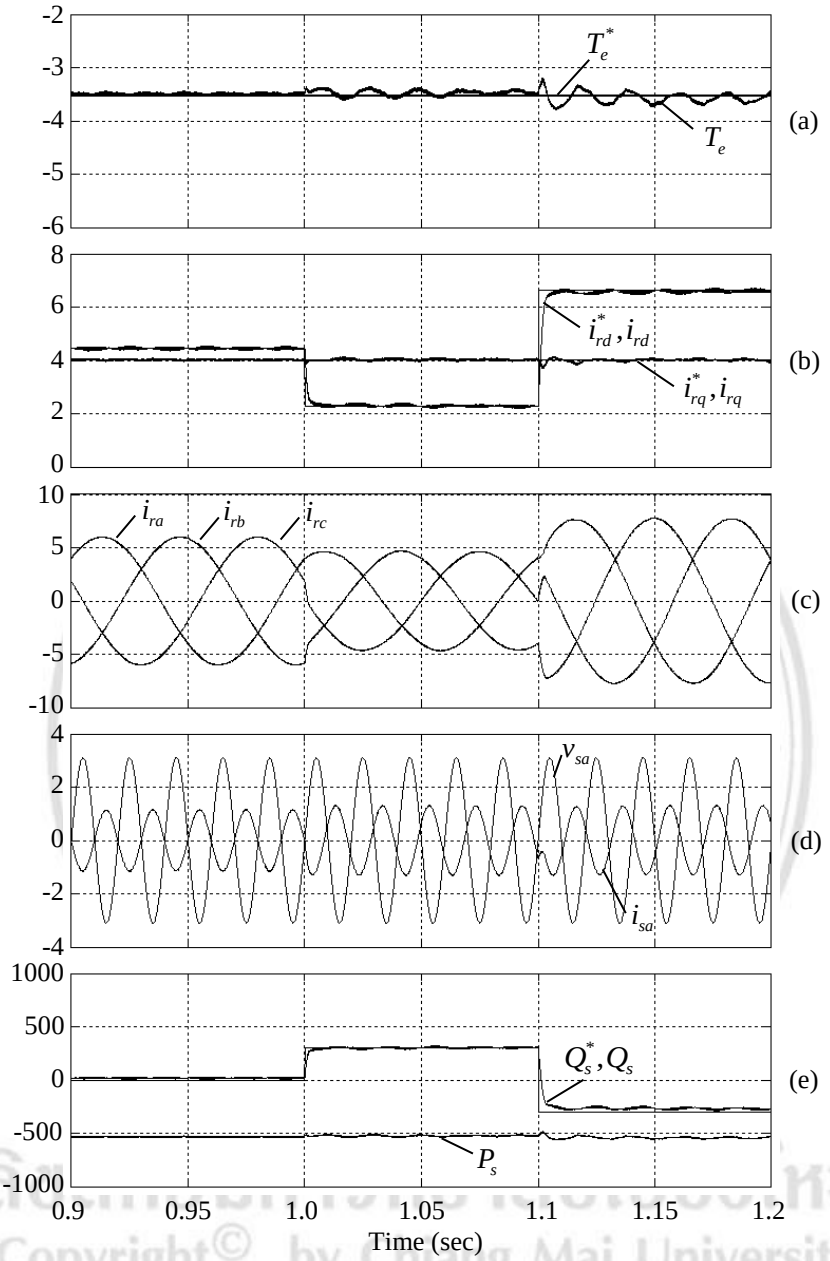

Figure 4.6 Simulation results under constant stator active power and various stator reactive power steps in constant sub-synchronous speed.

The simulated waveforms for the stator-side variables are shown in Figure 4.6 (d). For Q_s^* = 0 VAR, during the period of 0.9 < t < 1.0 s, the waveforms of the stator voltage v_{sa} and stator current i_{sa} are out of phase, which is operated in the generating mode with unity power factor. The stator active power delivered to the utility grid. When 1.0 < t < 1.1 s, the reactive power reference is changed to from zero to +300 VAR, as shown in Figure 4.6 (e),

demanding a lagging power factor operation. It can be seen that the stator current i_{sa} lags the stator voltage v_{sa}. The DFIG receipted the stator reactive power from the utility grid. After 1.1 s, the reference of the stator reactive power is changed to -300 VAR. The stator current i_{sa} leads the stator voltage v_{sa}, demanding a leading power factor operation. Finally, the DFIG system response during step change of reactive power is performed and the simulated results are shown in Figure 4.6 (e). The stator reactive power is step changed with from 0 VAR, +300 VAR, and -300 VAR, with the stator active power kept constant at 540 W.

4.4.2 Dynamic response in super-synchronous speed

The dynamic performance with super-synchronous constant speed at 1800 rpm and reactive power steps change has been carried out to simulate evaluate the dynamic response of the stator flux vector control scheme. This condition is generated by the constant torque command T_e^* for constant stator active power P_s, and the stator reactive power reference Q_s^* is set to 0 VAR for unity power factor and it is step changed from zero to +300 VAR at 1.0 s and from +300 to -300 VAR at 1.1 s, respectively. Simulation results are shown in Figure 4.7.

Figure 4.7 (a) shows the electromagnetic torque reference T_e^* and the electromagnetic torque of the generator T_e. It can be seen that the electromagnetic torque of generator is equal to the reference torque, around -5.3 Nm. Figure 4.7 (b) shows the rotor current reference components i_{rd}^*, i_{rq}^* and the measured rotor current components i_{rd}, i_{rq} in *d-q* rotating reference frame. It can be seen that the *d*-axis rotor current i_{rd} follows the rotor current reference i_{rd}^*, while the *q*-axis rotor current i_{rq} is maintained at its constant reference value i_{rq}^*. The three-phase rotor currents in sub-synchronous speed are shown in Figure 4.7 (c).

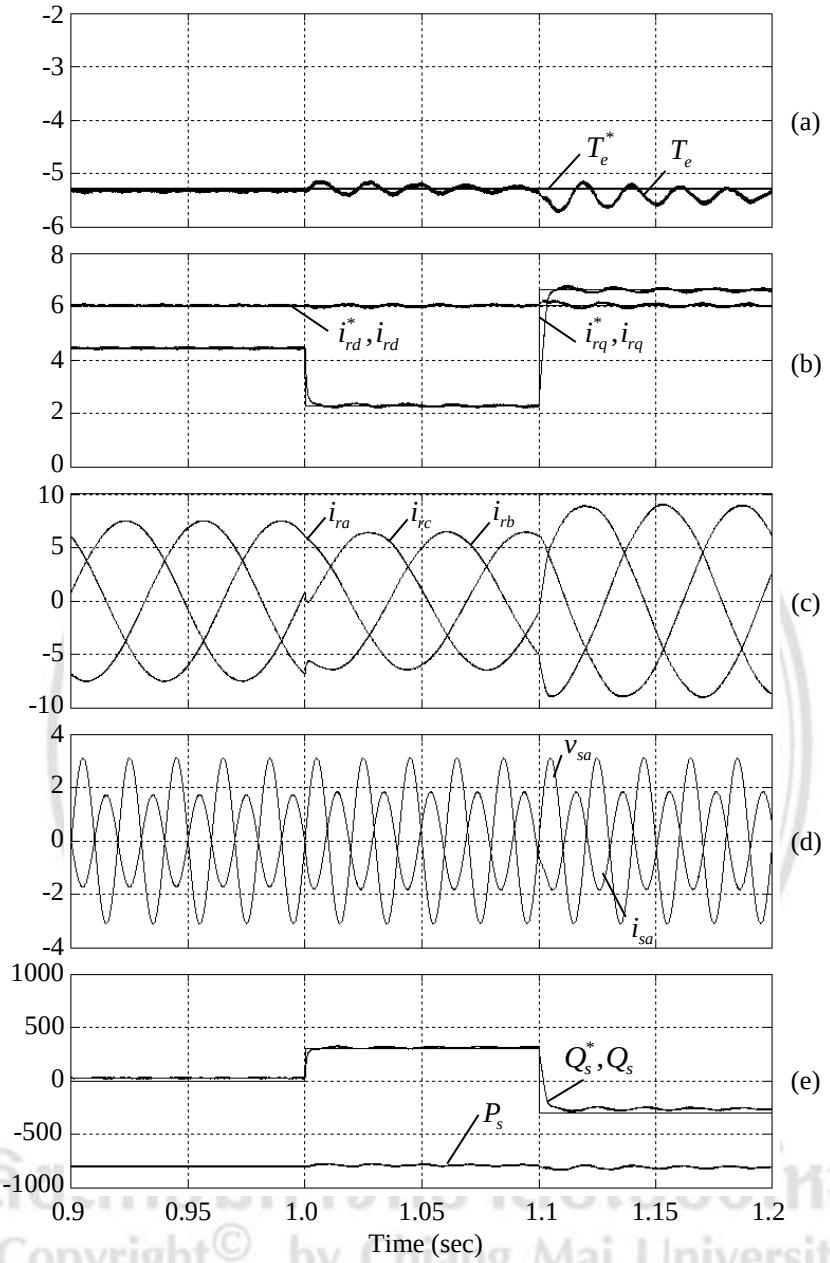

Figure 4.7 Simulation results under constant stator active power and various stator reactive power steps in constant super-synchronous speed.

Figure 4.7 (d), at lagging power factor operation, it can be seen that the stator current i_{sa} lags the stator voltage v_{sa}. The DFIG receipted the stator reactive power from the utility grid. After 1.1 s, the reference of the stator reactive power is changed to -300 VAR. The stator current i_{sa} leads the stator voltage v_{sa}, demanding a leading power factor operation. Finally, the simulated results during step change of the reactive power are shown in

Figure 4.7 (e). The stator reactive power is step changed with the stator active power kept constant at 795 W.

4.4.3 Dynamic response in speed change

The performance of the DFIG system is observed when varying the rotor speed from 1200 to 1800 rpm, rotor slip from $\pm 20\%$, as shown in Figure 4.8. Figures 4.8 (a) and (b) show the rotor speed n_r and slip angle θ_{sl} when the rotor speed is ramp up. Figure 4.8 (c) shows the electromagnetic torque reference T_e^* and the electromagnetic torque of the generator T_e. It can be seen that the electromagnetic torque of generator produced by rotor speed is equal to the reference torque. The waveform of rotor phase voltage v_{ra} and dc-link voltage v_{dc}, which is generated by the rotor-side converter, are shown in Figure 4.8 (d). It can be seen that the frequency of the rotor voltage is not constant. It is depending on the rotor speed. When the rotor operates at the synchronous speed (1500 rpm), the slip frequency is zero, the converter supplies a dc current to the generator while the dc-link voltage is also maintained by the grid-side converter. Figure 4.8 (e) shows the inverter phase voltage of grid-side converter v_{ia} together with the dc-link voltage v_{dc}. It can be observed that the frequency of the phase voltage is constant as utility grid frequency, 50 Hz. The three-phase rotor currents i_{ra}, i_{rb}, i_{rc} are shown in Figure 4.8 (f). It is clear that the rotor frequency changes as a function of the rotor slip. Figure 4.8 (f) shows the grid phase voltage v_{ga}, the stator current, i_{sa} and the grid current i_{ga}. It can be observed that the stator current i_{sa} is out of phase with its grid phase voltage v_{ga}. The stator active power delivered to the utility grid during sub- and super synchronous operations. However, it can be observed that the grid current i_{ga} is depending on the rotor speed, which affects the active power exchange between the rotor side converter. Therefore, the power exchange between the grid-side converter and the grid is different for sub- and super-synchronous operations.

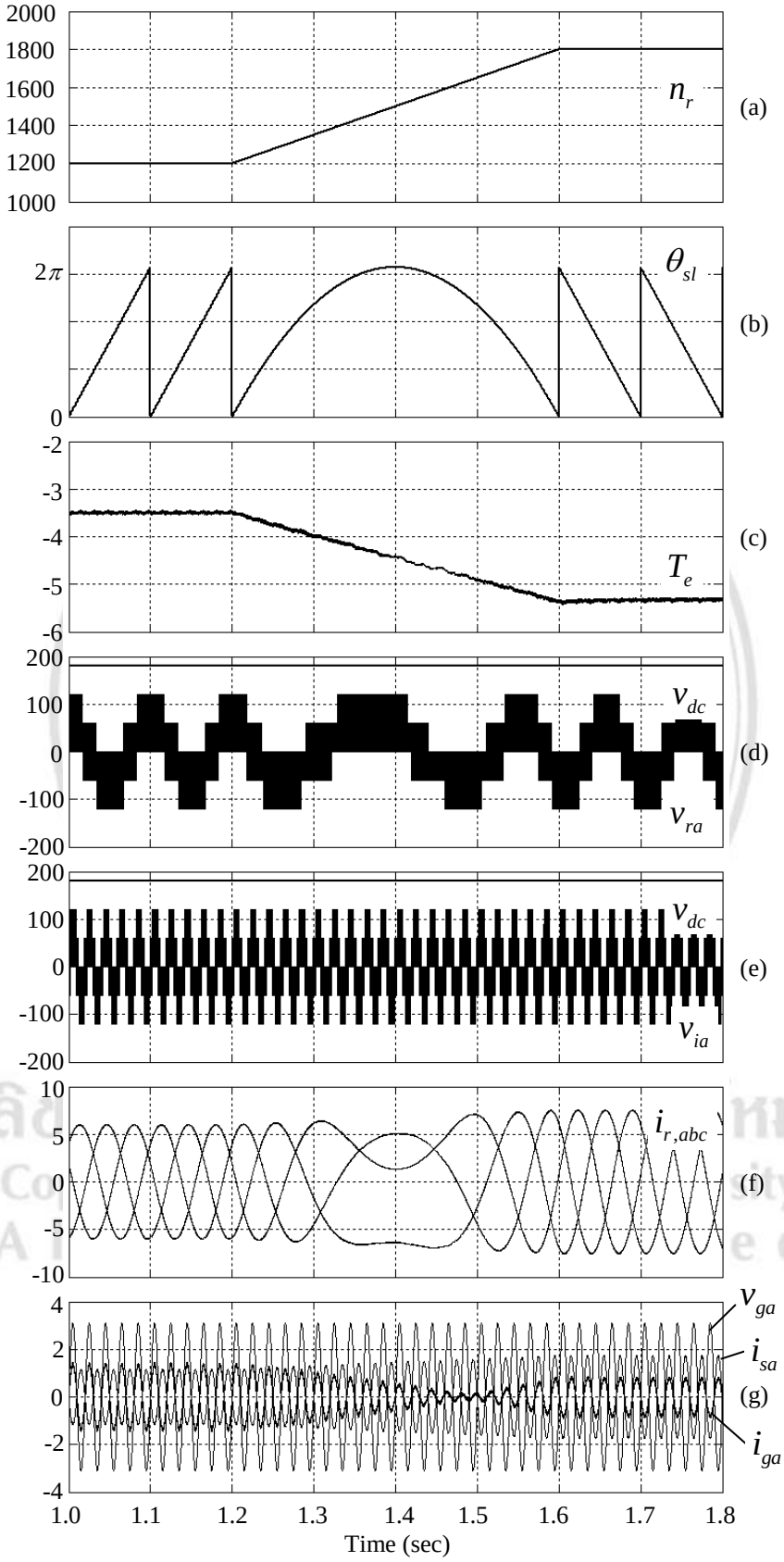

Figure 4.8 Simulation results under varying the stator active power during rotor speed variation.

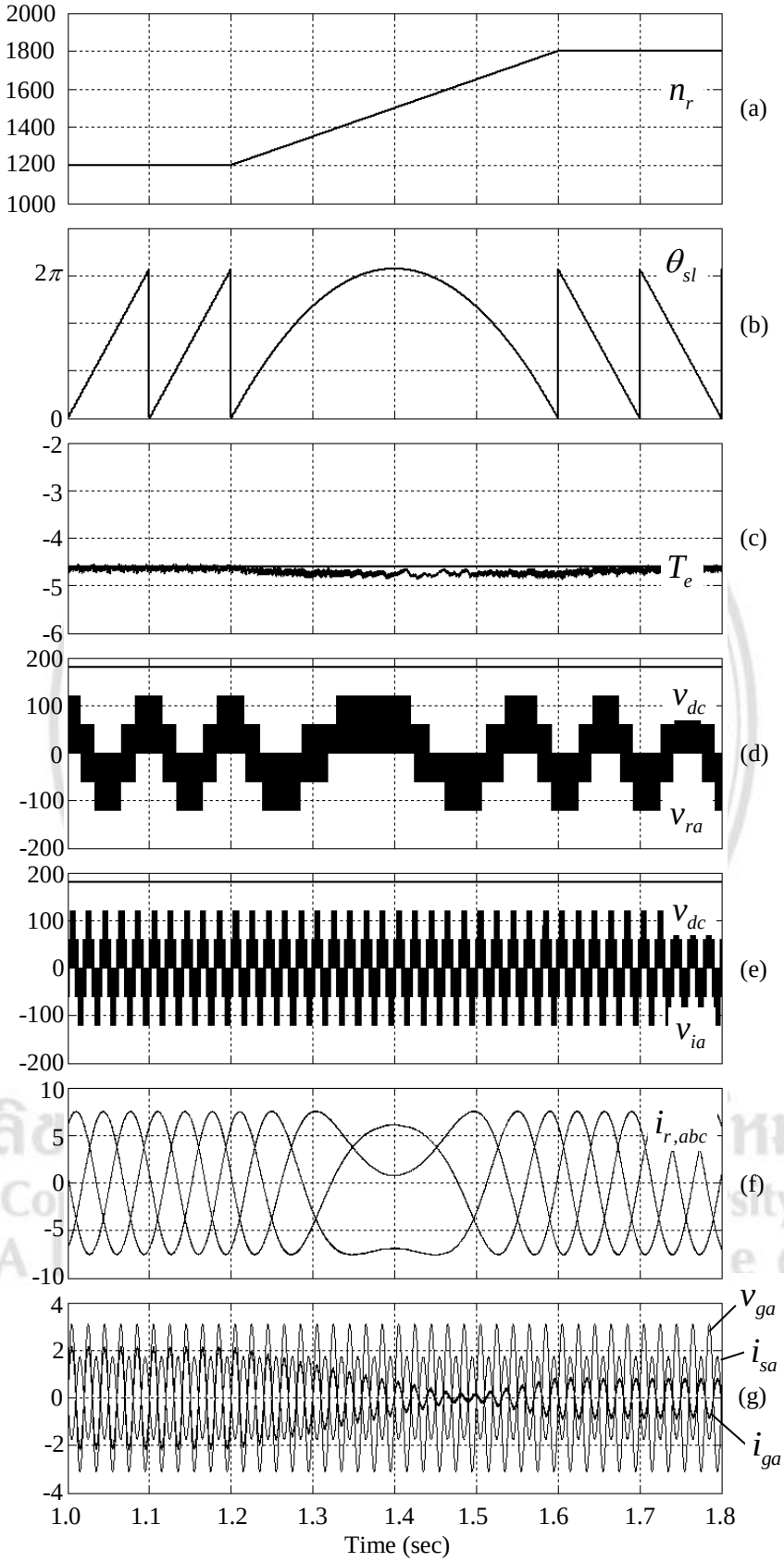

Figure 4.9 Simulation results under constant the stator active power during rotor speed variation.

The performance of the DFIG system is observed during varying the rotor speed change from 1200 to 1800 rpm, as shown in Figure 4.9. The stator active is constant at rated speed and the reactive power is set to zero. Figures 4.9 (a) and (b) show the rotor speed n_r and slip angle θ_{sl} when the rotor speed is ramp up. Figure 4.9 (c) shows the electromagnetic torque reference T_e^* and the electromagnetic torque of the generator T_e. It can be seen that the electromagnetic torque of generator is constant even under varying the rotor speed change. The waveform of rotor phase voltage v_{ra} and the dc-link voltage v_{dc}, which is generated by the rotor-side converter, are shown in Figure 4.9 (d). Figure 4.9 (e) shows the inverter phase voltage of grid-side converter v_{ia} together with the dc-link voltage v_{dc}. The three-phase rotor currents i_{ra}, i_{rb}, i_{rc} are shown in Figure 4.9 (f). It is clear that the rotor frequency changes as a function of the rotor slip. Figure 4.9 (g) shows the grid phase voltage v_{ga}, the stator current, i_{sa} and the grid current i_{ga}. From Figure 4.9, the dc-link voltage is also maintained by the grid-side controller. The difference of the grid phase current under speed change is due to the fact that the power consumption in the generator become opposite during sub- and super-synchronous speed operations.

Figure 4.10 shows the relationship between the mechanical power P_m, stator active power P_s, grid-side active power P_g and the total active power of the DFIG system P_t under speed change condition from 1200-1800 rpm. It can be seen that the variations of the active power are depending on the rotor speed. Finally, Figure 4.11 shows the active power waveforms under speed variation. These simulated waveforms are the same as Figure 4.10. It shows that the stator active power is kept constant during speed variation.

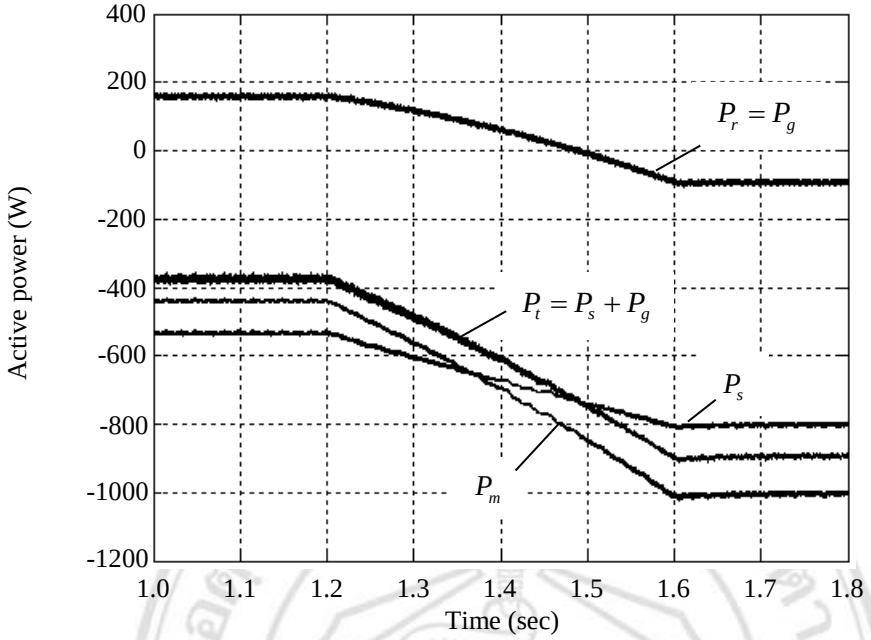

Figure 4.10 Simulation results of active power under speed change with stator active power variation.

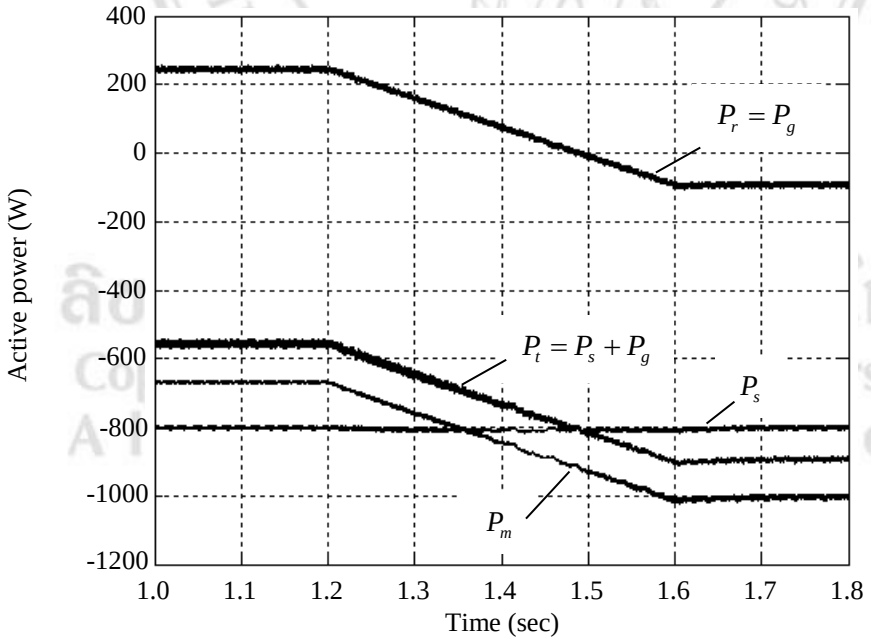

Figure 4.11 Simulation results of active power under speed change with stator active power constant.

4.5 Conclusion

In this chapter, the dynamic mathematical model and the stator flux vector control scheme of the DFIG system have been described. The DFIG system is controlled by the back-to-back two-level VSC. The rotor-side converter is controlled using stator flux vector control technique, which decouples the rotor currents into the stator active and reactive power, while the grid-side converter is controlled using grid voltage vector control technique. The simulation results verify the stator flux vector control scheme. The performance simulations show that this strategy is able to yield a good dynamic responses and high accuracy of the active and reactive power control. However, the disadvantage of stator flux vector control in the rotor-side converter controlled is the calculation of stator flux position. In addition, the two-level VSC requires switch with relatively high switching frequency. The switching losses are much higher than the devices conduction losses in particular to high power converters.